JCTC Journal of Chemical Theory and Computation

ARTICLE

pubs.acs.org/JCTC

How Well Can Modern Density Functionals Predict Internuclear Distances at Transition States?

Xuefei Xu, I. M. Alecu, and Donald G. Truhlar*

Department of Chemistry and Supercomputing Institute, University of Minnesota, Minneapolis, Minnesota 55455-0431, United States

ABSTRACT: We introduce a new database called TSG48 containing 48 transition state geometrical data (in particular, internuclear distances in transition state structures) for 16 main group reactions. The 16 reactions are the 12 reactions in the previously published DBH24 database (which includes hydrogen transfer reactions, heavy-atom transfer reactions, nucleophilic substitution reactions, and association reactions plus one unimolecular isomerization) plus four H-transfer reactions in which a hydrogen atom is abstracted by the methyl or hydroperoxyl radical from the two different positions in methanol. The data in TSG48 include data for four reactions that have previously been treated at a very high level in the literature. These data are used to test and validate methods that are affordable for the entire test suite, and the most accurate of these methods is found to be the multilevel BMC-CCSD method. The data that constitute the TSG48 database are therefore taken to consist of these very high level calculations for the four reactions where they are available and BMC-CCSD calculations for the other 12 reactions. The TSG48 database is used to assess the performance of the eight Minnesota density functionals from the M05−M08 families and 26 other high-performance and popular density functionals for locating transition state geometries. For comparison, the MP2 and QCISD wave function methods have also been tested for transition state geometries. The MC3BB and MC3MPW doubly hybrid functionals and the M08-HX and M06-2X hybrid meta-GGAs are found to have the best performance of all of the density functionals tested. M08-HX is the most highly recommended functional due to the excellent performance for all five subsets of TSG48, as well as having a lower cost when compared to doubly hybrid functionals. The mean absolute errors in transition state internuclear distances associated with breaking and forming bonds as calculated by the B2PLYP, MP2, and B3LYP methods are respectively about 2, 3, and 5 times larger than those calculated by MC3BB and M08-HX.

1. INTRODUCTION

Computational thermochemical kinetics is an important branch of theoretical chemistry focused on the prediction of thermal rate constants of chemical reactions. Reliable transition state properties (e.g., geometry and vibrational frequencies) and reaction barrier heights are indispensable information for calculating rate constants by transition state theory. Therefore, the reliability of the electronic structure method chosen for locating transition states and calculating their barrier heights will directly affect the quality of thermochemical kinetics calculations.

In the past 20 years, Kohn−Sham density functional theory (DFT) has become a workhorse of computational thermochemistry and thermochemical kinetics due to its lower computational cost compared to wave function theory (WFT) and to the continuing improvement of exchange-correlation functionals. However, the appropriate choice of functional is still a key issue for getting accurate results. Some benchmark databases[1−10] of barrier heights for diverse types of reactions have been established for the assessment of DFT functionals. DBH24/08[10] is of special interest because it was designed as a representative database, and it includes 24 accurate barrier heights for 12 reactions: three hydrogen transfer reactions, three heavy-atom transfer reactions, three nucleophilic substitution reactions of anions, and three unimolecular and association reactions. Recently, the DBH24/08 database was used[10] to assess 348 model chemistries. Several hybrid density functionals, in particular, M08-SO,[11] M06-2X,[12,13] M08-HX,[11] BB1K,[14] BMK,[15] PWB6K,[16] MPW1K,[17] BHandHLYP,[18c,d] and TPSS25B95,[19] were recommended for calculations of barrier heights.

Although considerable attention has been paid to the performance of DFT for barrier heights, the ability of density functionals to accurately calculate transition state geometries has been less well investigated. Inaccurate calculations of transition state geometries could lead to unrealistic potential energy surfaces, unreliable vibrational frequencies, and inaccurate predictions of rate constants and kinetic isotope effects. By 1998, it had already been learned that even the most successful functional (at that time), B3LYP,[18a,b,20] is quantitatively unreliable for transition state geometries and energies for a number of cases.[21] In 2001, the performance of four hybrid density functionals (MPW1K, mPW1PW91,[22] B3LYP, and BHandHLYP) was tested for predicting the transition state geometries of five reactions, as compared to very high-level calculations,[23] and only the MPW1K functional, which was optimized for kinetics, was recommended for locating transition state geometries. In 2005,[24] some newer DFT methods were tested for the transition state geometries and energetics of the hydrogen abstraction reaction from methanol by a hydrogen atom. The MC3BB doubly hybrid DFT method[25] and the BB1K hybrid meta-GGA, which was specially optimized for kinetics, were suggested as reasonably accurate DFT methods.

Since 2005, some new functionals have been developed, and we are especially concerned here with the Minnesota functionals,[26,27] which were designed for broad applicability in chemistry. As mentioned above, the Minnesota family of density

Received: February 14, 2011
Published: April 26, 2011

Table 1. The TSG48 Database

reactions		R_1	R_2	R_3
	HTG9: Hydrogen Transfer			
R1	$OH + CH_4 \rightarrow CH_3 + H_2O$	1.341	1.192	2.530
R2	$H + OH \rightarrow O + H_2$	0.894 (0.892)[a]	1.215 (1.216)[a]	2.109 (2.107)[a]
R3	$H + H_2S \rightarrow H_2 + HS$	1.160	1.426	2.578
	HATG9: Heavy-Atom Transfer			
R4	$H + N_2O \rightarrow OH + N_2$	1.431	1.226	2.187
R5	$H + ClH \rightarrow HCl + H$	1.480 (1.485)[a]	1.480 (1.485)[a]	2.960 (2.970)[a]
R6	$CH_3 + FCl \rightarrow CH_3F + Cl$	2.047	1.767	3.814
	NSG9: Nucleophilic Substitution of Anion			
R7	$Cl^- \cdots CH_3Cl \rightarrow ClCH_3 \cdots Cl^-$	2.305 (2.303)[a]	2.305 (2.303)[a]	4.610 (4.605)[a]
R8	$F^- \cdots CH_3Cl \rightarrow FCH_3 \cdots Cl^-$	2.020	2.114	4.134
R9	$OH^- + CH_3F \rightarrow HOCH_3 + F^-$	1.988	1.758	3.745
	UAG9: Unimolecular and Association			
R10	$H + N_2 \rightarrow HN_2$	1.439	1.127	2.201
R11	$H + C_2H_4 \rightarrow CH_3CH_2$	1.925	1.351	2.662
R12	$HCN \rightarrow HNC$	1.183 (1.188)[a]	1.387 (1.378)[a]	1.187 (1.194)[a]
	MHTG12: Methanol Hydrogen Transfer			
R13	$CH_3OH + HO_2 \rightarrow \cdot CH_2OH + HOOH$	1.240	1.289	2.501
R14	$CH_3OH + CH_3 \rightarrow \cdot CH_2OH + CH_4$	1.398	1.301	2.697
R15	$CH_3OH + HO_2 \rightarrow CH_3O\cdot + HOOH$	1.103	1.246	2.337
R16	$CH_3OH + CH_3 \rightarrow CH_3O\cdot + CH_4$	1.248	1.248	2.490

[a] For the cases where we use accurate values from refs 2 and 28, the BMC-CCSD value is given in parentheses for comparison.

functionals, especially the Minnesota 2008 functionals M08-HX and M08-SO, were found to perform well for calculating barrier heights.[10] Here, we test the performance of the Minnesota functionals and other popular (and a few interesting but not so popular) DFT functionals for calculating transition state geometries for a variety of reactions. To accomplish this, we present a database, called TSG48, of 48 data for transition state geometries.

2. TSG48 DATABASE

The 16 reactions in the TSG48 database are listed in Table 1. The database consists of five subdatabases: HTG9 for three hydrogen transfer reactions in DBH24, HATG9 for three heavy-atom transfer reactions in DBH24, NSG9 for three nucleophilic substitution reactions of anions in DBH24, UAG9 for three unimolecular and association reactions in DBH24, and MHTG12 for four H-transfer reactions in which an H atom is abstracted by the methyl or hydroperoxyl radical from the two different positions in methanol. For each reaction, we consider three geometrical data for transition state structures, in particular, three internuclear distances labeled R_1, R_2, and R_3. For each transition state, these are the three key distances involving the breaking and forming of bonds. For atom transfer reactions, A + X−D → A−X + D, where A is the acceptor, D is the donor, and X is the transferred atom; R_1, R_2, and R_3 are respectively the a−X, X−d, and a−d distances, where a is the accepting atom in the acceptor molecule or group A and d is the donating atom in the donor molecule or group D. For three S_N2 reactions, which are all methyl cation transfers, the three distances are a−C, C−d, and a−d, where C is the carbon of the methyl cation. For the R10 and R12 reactions, we consider all three distances with the order being H−N, N−N′, and N′−H for R10 and C−H, N−H, and C−N for R12. For reaction R11, namely, $H + C_2H_4 \rightarrow CH_3CH_2$, R_1, R_2, and R_3 are the three distances between the attached H atom and/or the two carbon atoms, with the order being H−C, C−C′, and C′−H.

Accurate transition state geometries[2,28] are available for four of the reactions (R2, R5, R7, and R12) in the TSG48 database. For reaction R2, the accurate values[28b] are based on an internally contracted multireference configuration interaction including all single and double excitations (with the 1s core of oxygen frozen) from a CASSCF reference space that was extended from the full-valence reference space by adding orbitals that are nominally 3pπ orbitals on O. The basis set was aug-cc-pVQZ. For reaction R5, the accurate values[28a] are based on internally contracted multireference configuration interaction including all single and double excitations (with the 1s, 2s, and 2p core electrons of Cl frozen) from a full-valence CASSCF reference space followed by scaling the external correlation-energy (SEC[28d]). The basis set was aug-cc-pV5Z, excluding h functions for Cl and aug-cc-pVQZ for H. They obtained an H−Cl bond length in the transition state of 1.480 Å, which is only 0.001 Å larger than an earlier[28e] calculation employing the SEC method with a smaller basis set. For reaction R7, the accurate values[2] are from CCSD(T)//cc-pVQZ+1 calculations. For reaction R12, the accurate values[28c] are based on the CCSD(T) method and exponential extrapolation to a complete basis set from optimizations with the cc-pCVDZ to cc-pCVQZ basis sets.

The four accurate values discussed in the previous paragraph were used to test the potential accuracy of nine wave function methods that have a lower cost than the methods used for the four accurate values. The nine wave function methods are multilevel BMC-CCSD,[29] the best N^6 method for barrier height calculations,[10] multireference second-order Møller−Plesset theory MRMP2[30] in combination with the MG3S[31] and aug-cc-pVTZ[32] basis sets,

Table 2. The Mean Unsigned Deviations MUD (in Å) of Transition State Geometries Obtained by Wave Function Methods for the Four Selected Reactions in TSG48 Database, Compared to the Best Estimated Geometries from refs 2 and 28

method	R2[a]	R5[b]	R7[c]	R12[d]	AMUD[e]
BMC-CCSD	0.002	0.007	0.003	0.007	0.005
MRMP2/*nom*-CPO/MG3S[40]	0.011	0.003	0.004	0.009	0.007
QCISD/MG3	0.017	0.008	0.023	0.003	0.013
MP2/6-31+G(d,p)	0.018	0.013	0.008	0.021	0.015
MRMP2/*nom*-CPO/aug-cc-pVTZ[40]	0.016	0.003	0.038	0.008	0.016
MP2/def2-TZVP	0.019	0.013	0.028	0.013	0.018
MP2/MG3S	0.024	0.016	0.023	0.013	0.019
MP2/ma-TZVP	0.020	0.017	0.027	0.013	0.019
MP2/maug-cc-pV(T+d)Z	0.022	0.027	0.038	0.016	0.026

[a] Accurate values from ref 28b. [b] Accurate values from ref 28a. [c] Accurate values from ref 2. [d] Accurate values from ref 28c. [e] Average deviation from 12 accurate transition state internuclear distances.

quadratic configuration interaction with single and double excitations[33] (QCISD with the MG3[31a−e,34] basis set), and second-order Møller−Plesset theory[35] (MP2) with five different basis sets: MG3S, ma-TZVP,[36] def2-TZVP,[37] maug-cc-pV(T+d)Z,[32,38] and 6-31+G(d,p).[39] The tests are given in Table 2. The mean unsigned deviation (MUD, where the deviation is the difference from the accurate value) of the three key bond lengths R_1, R_2, and R_3 for each of the four reactions are given in the table, which also shows the average MUD (AMUD) in the three internuclear distances over the four reactions for each wave function method. Table 2 shows that the BMC-CCSD method gives the most accurate transition state structures with an AMUD of only 0.005 Å, and it even performs better than MRMP2 using nominal correlated participating orbitals (*nom*-CPO) as an active space in combination with the MG3S basis set, as reported in a previous study.[40] It also performs better than the more expensive QCISD/MG3 method. The MP2 method is sensitive to the basis set, and its combination with 6-31+G(d,p) gives good results, which are comparable with those obtained by the MRMP2/*nom*-CPO/aug-cc-pVTZ method.[40] However, it is broadly appreciated that the tendency of MP2 to give better results with small basis sets results from a cancellation of errors.

As a result of its good performance in the test of Table 2, we shall use BMC-CCSD geometries for the other 12 reactions. All 36 geometrical data for the 12 reactions obtained by BMC-CCSD and 12 geometrical data from the literature for the four reactions with accurate values are shown in Table 1, and the 48 geometrical data constitute the TSG48 database. For comparison, the BMC-CCSD results for the four reactions with accurate values are also shown in Table 1.

3. COMPUTATIONAL DETAILS

For both wave function and density functional methods, the transition state geometries of the 16 reactions in TSG48 have been located and confirmed by frequency calculations. The wave function methods employed include MP2, QCISD, and BMC-CCSD, and the DFT functionals include four generalized gradient approximations (GGAs), MOHLYP,[41] MOHLYP2,[10] BLYP,[18a,b] and SOGGA;[42] one meta-GGA, M06-L;[12,26] 12 hybrid GGAs, ωB97,[43] ωB97X,[43] ωB97X-D,[44] MPW1K, PBE0,[45] mPW1PW,[22] B97-3,[46] B97-D,[47] B98,[48] B1LYP,[49] BHandHLYP, and B3LYP; 14 hybrid meta-GGAs: M08-HX, M08-SO, M06-2X, PWB6K, BB1K, MPWB1K,[50] PW6B95,[16] BMK, TPSS25B95, M05-2X,[51] M06-HF,[52] M06,[13] M05,[53] and τHCTHhyb;[54] and three doubly hybrid functionals, MC3BB, MC3MPW,[25] and B2PLYP.[55] Note that the hybrid GGAs may be further classified: MPW1K, PBE0, mPW1PW, B97-3, B98, B1LYP, BHandHLYP, and B3LYP are global hybrid GGAs; B97-D is a global hybrid GGA combined with molecular mechanics; ωB97 and ωB97X are range-separated hybrid GGAs; and ωB97X-D is a range-separated hybrid GGA combined with molecular mechanics. Note that hybrid and doubly hybrid functionals include a nonzero percentage of Hartree−Fock exchange, and other functionals do not; the latter functionals are called local and are less expensive for geometry optimizations of large systems.

The MG3S basis set has been used for all DFT and MP2 calculations except for BMC-CCSD, MC3BB, and MC3MPW, in which particular basis sets are specified for the components in these calculations by the definitions of the methods. For the QCISD calculations, in which the transition state geometries of the 12 reactions in DBH24 are taken from ref 8, the MG3 basis set was used. Other basis sets, in particular, ma-TZVP, def2-TZVP, maug-cc-pV(T+d)Z, and 6-31+G(d,p), have also been tested for several selected functionals to confirm that MG3S is a good choice for the optimization of transition state geometries.

For some model chemistries, the exoergic direction of some reactions, in particular R6, R8, and R15, appears to proceed without a barrier. In such cases, the energetic transition state is technically predicted to be located at the reactant asymptote by that model chemistry, and the error in some of the internuclear distances is therefore infinite. Thus, we could have listed the mean error for such model chemistries as infinite, but we thought it would be more informative to assign a large finite error in such cases. Therefore, for such bond lengths, in order to compute the MUD, the deviation was set not to infinity but rather to the largest deviation for that bond length in any of the model chemistries that have a finite error for that bond length.

All calculations were performed using Gaussian09.a02,[56] Gaussian03.d01,[57] or a locally modified version of Gaussian03.e01. MNGFM4.1[58] that contains additional Minnesota functionals. For the multilevel BMC-CCSD and doubly hybrid MC3BB and MC3MPW methods, the MLGauss2.0[59] program was used.

Note that all transition states discussed in this article are conventional transition states, i.e., saddle points, not variational transition states.

4. RESULTS AND DISCUSSION

Table 3 shows the average MUD in the three internuclear distances of transition state geometries as compared to the ones in the TSG48 database for each of the five subsets: HTG9, HATG9, NSG9, UAG9, and MHTG12. All density functional results in Table 3 were obtained with the MG3S basis set (except for the MC3BB and MC3MPW results, as discussed above). Table 3 also gives the AMUDs over all 48 geometrical data in TSG48. For comparison, the AMUDs for the MP2/MG3S and QCISD/MG3 methods are also included in Table 3.

4.1. The Performance over the 16 Reactions of TSG48. Overall, the MC3BB doubly hybrid functional, the M08-HX hybrid meta-GGA, and the MC3MPW doubly hybrid functional perform best when all 16 reactions in TSG48 are considered.

Table 3. The Average Mean Unsigned Deviations (AMUD, in Å) of Transition State Geometries Obtained Using 36 Model Chemistries, Compared to the TSG48 Database

method	type[a]	HTG9	HATG9	NSG9	UAG9	MHTG12	**TSG48**	TSG39[b]
QCISD/MG3	WFT	0.020	0.013	0.015	0.014	0.014	**0.015**	0.014
MP2/MG3S	WFT	0.038	0.067	0.017	0.041	0.025	**0.037**	0.034
MC3BB	DHDFT	0.011	0.020	0.009	0.018	0.009	**0.013**	0.013
M08-HX/MG3S	H-m	0.016	0.012	0.013	0.016	0.014	**0.014**	0.015
MC3MPW	DHDFT	0.012	0.027	0.012	0.023	0.009	**0.016**	0.015
M06-2X/MG3S	H-m	0.021	0.013	0.017	0.025	0.012	**0.017**	0.018
M08-SO/MG3S	H-m	0.018	0.022	0.030	0.017	0.020	**0.021**	0.020
ωB97/MG3S	H	0.030	0.025	0.013	0.034	0.011	**0.022**	0.023
PWB6K/MG3S	H-m	0.028	0.022	0.015	0.031	0.021	**0.023**	0.024
B2PLYP/MG3S	DHDFT	0.019	0.029	0.042	0.017	0.015	**0.024**	0.018
BB1K/MG3S	H-m	0.030	0.024	0.014	0.038	0.018	**0.025**	0.025
ωB97X/MG3S	H	0.034	0.026	0.014	0.040	0.013	**0.025**	0.025
MPWB1K/MG3S	H-m	0.029	0.022	0.018	0.037	0.019	**0.025**	0.026
M05-2X/MG3S	H-m	0.041	0.022	0.015	0.056	0.006	**0.027**	0.028
BMK/MG3S	H-m	0.034	0.039	0.013	0.039	0.016	**0.028**	0.027
MPW1K/MG3S	H	0.029	0.021	0.018	0.058	0.017	**0.028**	0.030
ωB97X-D/MG3S	H	0.036	0.035	0.021	0.046	0.015	**0.030**	0.029
BHandHLYP/MG3S	H	0.043	0.023	0.023	0.051	0.021	**0.032**	0.031
M06-HF/MG3S	H-m	0.044	0.019	0.045	0.030	0.032	**0.034**	0.035
PW6B95/MG3S	H-m	0.038	0.048	0.025	0.045	0.021	**0.034**	0.030
PBE0/MG3S	H	0.037	0.041	0.016	0.068	0.023	**0.036**	0.033
M06/MG3S	H-m	0.044	0.047	0.033	0.051	0.016	**0.037**	0.033
mPW1PW/MG3S	H	0.036	0.042	0.021	0.068	0.022	**0.037**	0.033
TPSS25B95/MG3S	H-m	0.048	0.050	0.032	0.043	0.024	**0.038**	0.031
B97-3/MG3S	H	0.039	0.045	0.034	0.053	0.024	**0.038**	0.035
M05/MG3S	H-m	0.042	0.048	0.041	0.078	0.021	**0.044**	0.040
B98/MG3S	H	0.058	0.076	0.047	0.071	0.028	**0.054**	0.046
B1LYP/MG3S	H	0.059	0.071	0.066	0.069	0.024	**0.056**	0.049
B3LYP/MG3S	H	0.065	0.095	0.069	0.080	0.029	**0.065**	0.054
M06-L/MG3S[c]	m	0.070	0.100	0.069	0.081	0.039	**0.070**	0.057
τHCTHhyb/MG3S[c]	H-m	0.084	0.107	0.059	0.087	0.040	**0.073**	0.058
SOGGA/MG3S[d]	GGA	0.132	0.032	0.043	0.159	0.069	**0.086**	0.091
MOHLYP2/MG3S	GGA	0.074	0.101	0.199	0.056	0.072	**0.099**	0.082
BLYP/MG3S[c,d,e]	GGA	0.163	0.125	0.148	0.133	0.065	**0.123**	0.108
MOHLYP/MG3S[c,d]	GGA	0.205	0.117	0.126	0.137	0.076	**0.129**	0.121
B97-D/MG3S[c,d,e]	H	0.285	0.117	0.149	0.168	0.054	**0.148**	0.140

[a] Abbreviations: WFT, wave function theory; DHDFT, doubly hybrid DFT; H-m, hybrid meta-GGA; H, hybrid GGA; m, meta-GGA; GGA, generalized gradient approximation. [b] TSG39 is the same as TSG48 except that R6, R8, and R15 are omitted. [c] The transition state of reaction R6 cannot be located. The largest deviations of the three key bond lengths obtained using other model chemistries were used to calculate the MUD in such cases. [d] The transition state of reaction R15 cannot be located. The largest deviations of the three key bond lengths obtained using other model chemistries were used to calculate the MUD in such cases. [e] The transition state of reaction R8 cannot be located. The largest deviations of the three key bond lengths obtained using other model chemistries were used to calculate the MUD in such cases.

First, we consider the two doubly hybrid DFT methods. MC3BB performs best of all; it does even better than the more expensive QCISD/MG3 method. MC3BB includes kinetic energy density, while MC3MPW does not. Thus, MC3MPW would be an alternative choice for users of computer programs that do not include functionals with kinetic energy density. The third doubly hybrid DFT method we tested, B2PLYP, does not perform as well as either MC3BB or MC3MPW. The MP2 components in MC3BB and MC3MPW are obtained with the basis set 6-31+G(d,p), which has been found to yield better results than MG3S in section 2. This could be one of the reasons that MC3-type methods do better than B2PLYP/MG3S, although a more likely reason is that MC3BB and MC3MPW are parametrized for use with specific basis sets. Incidentally, we note that a timing analysis in which the relative computational cost associated with MC3BB, MC3MPW, and B2PLYP/MG3S was estimated by taking the average of the total CPU times required for the single-point energy calculation of each of the four transition states in reactions 13−16, and dividing this quantity by exactly the same quantity obtained from HF/MG3S single-point calculations, using the same computational software and the same computer, revealed that these three model chemistries have comparable computational costs for single-point energies—each being on average 3−4 times more expensive than HF/MG3S. However, for

geometry optimization, the more relevant cost is that for a single-point gradient, by which we mean a gradient at a single geometry (this includes the computer time to calculate one energy and a gradient at the same geometry as the energy), and a comparison like that just described, but for single-point gradients, reveals that MC3BB, MC3MPW, and B2PLYP/MG3S single-point gradients are respectively 4.6, 3.9, and 4.5 times more expensive (averaged over the four transition states) than single-point HF/MG3S gradients.

Most of the hybrid meta-GGAs predict better transition state geometries than GGAs and hybrid GGAs. The two best hybrid meta-GGAs are M08-HX and M06-2X, and their AMUDs are 0.014 Å and 0.017 Å, respectively, over the 16 reactions, which is similar in quality to MC3BB and MC3MPW. The range-separated ωB97 functional is the best hybrid GGA we tested. Twelve hybrid meta-GGAs (M08-HX, M06-2X, M08-SO, PWB6K, BB1K, MPWB1K, M05-2X, BMK, PW6B95, M06-HF, M06, and TPSS25B95) and eight hybrid GGAs (ωB97, ωB97X, MPW1K, ωB97X-D, BHandHLYP, PBE0, mPW1PW, and B97-3) have a better or similar performance to that of MP2 with the MG3S basis set, but with less cost. The hybrid B3LYP functional is very widely used but is found to perform poorly here.

The τHCTHhyb and B97-D functionals are respectively the worst hybrid-meta GGA and worst hybrid GGA for the 16 reactions explored here. These two functionals, along with the GGA functionals we tested, are not good enough for reliable optimizations of transition state geometries; some transition states for reactions (R6, R8, and R15) with low reaction barriers cannot even be located successfully because, when using the functionals mentioned above, there is no barrier. The M06-L meta-GGA performs better than any other tested functional that has no Hartree−Fock exchange. MOHLYP2 is the only GGA that can locate all transition state structures for the 16 reactions explored here, although it has a large AMUD.

4.2. The Performance for the Subsets of TSG48. For the hydrogen atom transfer reactions in HTG9, the superiority of the doubly hybrid DFT methods is especially remarkable, and all three doubly hybrid methods, namely, MC3BB, MC3MPW, and B2PLYP, perform better than QCISD/MG3. The three best hybrid meta-GGAs (M08-HX, M06-2X, and M08-SO) have similar performance to the more expensive B2PLYP.

Due to the worse performance of the MP2 component, the doubly hybrid DFT methods give worse results than many hybrid meta-GGAs for the heavy atom transfer reactions of HATG9. In this case, M08-HX, QCISD/MG3, and M06-2X become the three best methods. M06-HF and SOGGA are found to perform better in HATG9 than in other subsets; M06-HF gives a better result than doubly hybrid functionals for this subset.

Many of the model chemistries tested in the present work are suitable for locating the transition states of the anionic nucleophilic substitution reactions in NSG9. Again, MC3BB and MC3MPW perform better than QCISD/MG3, and MP2/MG3S is almost as good. It is perhaps surprising to find that B2PLYP has poor performance for this subset; the relatively poor behavior of B2PLYP in predicting barrier heights for nucleophilic substitution reactions[10] could be the main reason.

None of the DFT methods perform better than QCISD/MG3 for the UAG9 subset (unimolecular and association reactions). Most of the density functionals tested have the worst performance for this subset; this could result from the transition states of the reactions in UAG9 all having significant multireference character.[40] The four best DFT methods over these three reactions are M08-HX, M08-SO, B2PLYP, and MC3BB. M06-2X, which is usually among the top performers for other reaction types, performs relatively worse but still reasonably well. Other functionals with performances significantly above average for this difficult set are MC3MPW, M06-HF, and PWB6K.

All DFT-based electronic model chemistries performed relatively well for the hydrogen transfer reactions from methanol to the methyl or hydroperoxyl radicals in the MHTG12 subset, except for the GGA methods. Hydrogen bonding plays an important role in stabilizing the transition states for R13 and R15. The best performance for the MHTG12 subset is for M05-2X (which is reasonably accurate for systems characterized by hydrogen bonding and other weak noncovalent interactions[13]), which attains an AMUD of just 0.006 Å.

4.3. Dependence on Basis Set. In this section, we consider the dependence of the results on basis set. The goal is not a study of basis set convergence (where one might, for example, systematically look at changes in going from double-ζ to triple-ζ to quadruple-ζ in a convergent sequence of basis sets) but rather a study of how accurate the results are when one uses the basis sets that have become popular because of their favorable general performance/cost ratio and their affordability for large systems. Such basis sets are of special interest because they have stood the test of being widely applied, which in practice is a form of broad testing. This is necessarily unsystematic because these broadly tested basis sets are not themselves systematic, but we chose basis sets for the present study on the basis of our previous experiences in basis set selection for transition state calculations, for example refs 10, 36, and 38b.

MG3S is a minimally augmented triple-ζ basis set that is highly recommended for kinetics based on our previous studies. However the double-ζ 6-31+G(d,p) basis set was found to be a better basis set for the MP2 method for four reactions discussed in section 2 due to cancellation of errors. It is well-known that MP2 results often become worse as the basis set is increased, and similar deterioration is often seen for density functional calculations using relatively inaccurate functionals, such as B3LYP. Thinking along these lines, one might ask which double- or triple-ζ basis set is most suitable for density functional studies of transition state geometry and how much does the quality of the result depend on the specific choice of basis. To answer this, MG3S, 6-31+G(d,p), and three additional triple-ζ basis sets, def2-TZVP, ma-TZVP, and maug-cc-pV(T+d)Z, were tested for selected methods (MP2, B2PLYP, M08-HX, M06-2X, MPW1K, B3LYP, and τHCTHhyb) over the 12 reactions in the DBH24 database. The 6-31+G(d,p) basis set is chosen for this study because we and others have found for numerous applications that it is a good general choice for DFT calculations at the double-ζ level. The ma-TZVP and maug-cc-pV(T+d)Z basis sets are chosen because they are examples of minimally augmented basis sets, which have been highly recommended for general applications of DFT.[36,38b,60,61] The ma-TZVP basis set is a modification of the def2-TZVP basis set[37] minimally augmented by one diffuse s function and one diffuse p subshell on all non-hydrogenic atoms. The maug-cc-pV(T+d)Z basis set is the aug-cc-pV(T+d)Z basis set with the set of diffuse basis functions truncated to only the s and p functions on non-hydrogenic atoms. The corresponding calculated average mean unsigned deviations (AMUDs) for these basis sets for the TSG48 database are shown in Table 4.

Table 4 provides yet another example where MP2's performance is not improved by using better basis sets, and the best results are obtained with the smallest basis set examined. Since it is known that

Table 4. The Average Mean Unsigned Deviations (AMUD, in Å) of Transition State Geometries Obtained Using MP2 and Six DFT Methods in Combination with Five Basis Sets, for Subdatabases of the TSG48 Database

method	HTG9	HATG9	NSG9	UAG9	TSG36[a]	TSG30[a]
M06-2X/MG3S	0.021	0.013	0.017	0.025	0.019	0.020
M06-2X/ma-TZVP	0.024	0.011	0.014	0.025	0.019	0.020
M06-2X/def2-TZVP	0.025	0.013	0.020	0.024	0.021	0.021
M06-2X/maug-cc-pV(T+d)Z	0.021	0.012	0.014	0.028	0.019	0.020
M06-2X/6-31+G(d,p)	0.030	0.036	0.022	0.035	0.031	0.029
M08-HX/MG3S	0.016	0.012	0.013	0.016	0.014	0.014
M08-HX/ma-TZVP	0.018	0.011	0.012	0.017	0.015	0.015
M08-HX/def2-TZVP	0.019	0.013	0.008	0.017	0.014	0.016
M08-HX/maug-cc-pV(T+d)Z	0.018	0.010	0.013	0.019	0.015	0.015
M08-HX/6-31+G(d,p)	0.021	0.029	0.017	0.021	0.022	0.021
B3LYP/MG3S	0.065	0.095	0.069	0.080	0.077	0.061
B3LYP/ma-TZVP	0.072	0.082	0.068	0.081	0.076	0.063
B3LYP/def2-TZVP[b]	0.076	0.079	0.107	0.079	0.085	0.064
B3LYP/maug-cc-pV(T+d)Z	0.069	0.083	0.064	0.084	0.075	0.063
B3LYP/6-31+G(d,p)[c]	0.081	0.119	0.087	0.106	0.098	0.080
MPW1K/MG3S	0.029	0.021	0.018	0.058	0.032	0.033
MPW1K/ma-TZVP	0.035	0.018	0.020	0.059	0.033	0.035
MPW1K/def2-TZVP	0.037	0.017	0.028	0.058	0.035	0.036
MPW1K/maug-cc-pV(T+d)Z	0.030	0.019	0.020	0.062	0.033	0.035
MPW1K/6-31+G(d,p)	0.038	0.035	0.019	0.071	0.041	0.039
τHCTHhyb/MG3S[c]	0.084	0.107	0.059	0.087	0.084	0.065
τHCTHhyb/ma-TZVP[c]	0.088	0.107	0.057	0.088	0.085	0.066
τHCTHhyb/def2-TZVP[b,c]	0.088	0.108	0.097	0.087	0.095	0.067
τHCTHhyb/maug-cc-pV(T+d)Z[b]	0.086	0.106	0.053	0.089	0.084	0.066
τHCTHhyb/6-31+G(d,p)[b]	0.104	0.119	0.075	0.105	0.101	0.083
B2PLYP/MG3S	0.019	0.029	0.042	0.017	0.026	0.020
B2PLYP/ma-TZVP	0.019	0.025	0.039	0.016	0.025	0.019
B2PLYP/def2-TZVP	0.022	0.025	0.054	0.015	0.029	0.020
B2PLYP/maug-cc-pV(T+d)Z	0.020	0.025	0.034	0.020	0.025	0.020
B2PLYP/6-31+G(d,p)	0.025	0.051	0.055	0.026	0.039	0.030
MP2/MG3S	0.038	0.067	0.017	0.041	0.041	0.036
MP2/ma-TZVP	0.037	0.069	0.018	0.041	0.042	0.036
MP2/def2-TZVP	0.037	0.066	0.026	0.042	0.043	0.036
MP2/maug-cc-pV(T+d)Z	0.037	0.073	0.028	0.039	0.044	0.038
MP2/6-31+G(d,p)	0.033	0.051	0.012	0.032	0.032	0.028

[a] TSG36 is the same as TSG48 except that R13−R16 are omitted; TSG30 is the same as TSG36 except that R6 and R8 are omitted. [b] The transition state of reaction R8 cannot be located. The largest deviations of the three key bond lengths obtained using other model chemistries were used to calculate the MUD in such cases. [c] The transition state of reaction R6 cannot be located. The largest deviations of the three key bond lengths obtained using other model chemistries were used to calculate the MUD in such cases.

MP2 requires large basis sets for convergence of energies, this clearly results from a cancellation of errors. However, density functional theory does not benefit from such cancellation, and the double-ζ basis set 6-31+G(d,p) is clearly not good enough for reliable density functional calculations of transition state geometries. All four triple-ζ basis sets studied in Table 4 have similar performances for the typical density functionals when the R6 and R8 reactions are excluded. B3LYP and τHCTHhyb failed to locate the transition state with the less diffuse def2-TZVP basis set for reaction R8, and B3LYP/6-31+G(d,p) also failed for R6. The functionals with relatively poor performance for barrier heights need more diffuse and larger basis sets.

Table 4 shows that MG3S, maug-cc-pV(T+d)Z, and ma-TZVP are equally well suited for DFT studies of transition state geometries. This confirms the reasonableness of using the MG3S basis set in the tests in Table 3 for evaluating the performance of density functionals.

4.4. The Relationship between Good Performance for Barrier Heights and That for Transition State Geometries. On the basis of the present investigation, the hybrid functionals that were recommended for the calculations of barrier heights,[10] M08-HX, M08-SO, M06-2X, BB1K, BMK, PWB6K, MPW1K, BHandHLYP, and TPSS25B95, can all obtain comparable or more reliable transition state geometries than those obtained by MP2. Figure 1 provides a more thorough test of the question: is good performance for locating transition state geometries associated with smaller errors for barrier heights? Figure 1 includes all methods applied to the entire TSG48 database in this article that were also evaluated for predicting barrier heights in the DBH24/08 article,[10] except that the methods that failed to

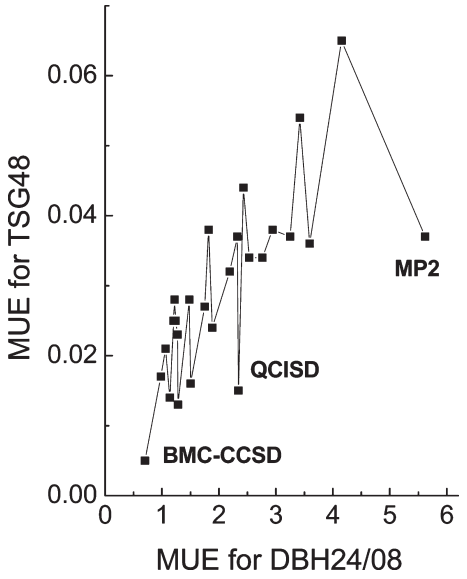

Figure 1. Plot of MUE (in Å) for TSG48 vs MUE (in kcal/mol) for DBH24/08 for various methods. The three results for wave function methods are labeled, and the unlabeled points all correspond to density functional theory. From left to right, the complete set of points corresponds to BMC-CCSD, M06-2X/MG3S, M08-SO/MG3S, M08-HX/MG3S, BB1K/MG3S, BMK/MG3S, MPWB1K/MG3S, PWB6K/MG3S, MC3BB, MPW1K/MG3S, MC3MPW, M05-2X/MG3S, B97-3/MG3S, B2PLYP/MG3S, BHandHLYP/MG3S, M06/MG3S, QCISD/MG3, M05/MG3S, M06-HF/MG3S, PW6B95/MG3S, TPSS25B95/MG3S, mPW1PW/MG3S, B98/MG3S, PBE0/MG3S, B3LYP/MG3S, and MP2/MG3S. Since the BMC-CCSD data are used as reference data for part of TSG48, the value plotted is based on only the reactions where a more accurate value is available; that is, it is based on Table 2 or 5, whereas the other values in the plot are based on Table 3.

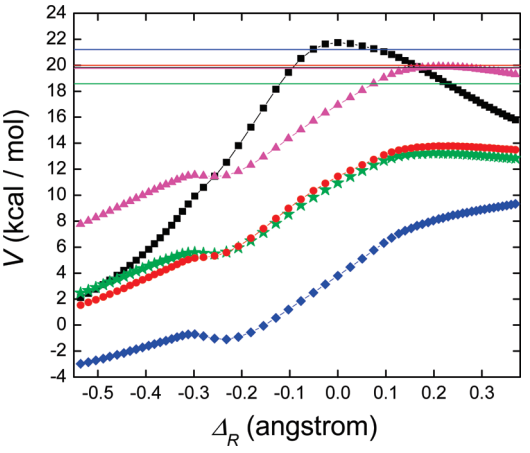

Figure 2. Potential energy curves $V(\Delta_R)$ for reaction R15 generated by single-point energy calculations along a fixed reaction path. For all five curves, the reaction path is the M08-SO/MG3S minimum-energy path in isoinertial coordinates, and Δ_R is a measure of the reaction progress defined in the text. The curves correspond to five different density functional methods: BLYP/MG3S (green stars), B97-D/MG3S (red circles), SOGGA/MG3S (blue diamonds), MOHLYP/MG3S (magenta triangles), and M08-SO/MG3S (black squares). In each case, the potential curve is normalized relative to its value for the reactants at the M08-SO/MG3S geometry. The value of the reaction energy (to which each curve would tend if extended to the right) are also shown for each of the five density functional methods, in corresponding colors; these values are calculated, for the purposes of this figure, by using the M08-SO/MG3S geometries for the reactants and products in all cases and have values of 18.57, 20.00, 21.20, 19.76, and 19.81 kcal/mol for BLYP/MG3S, B97-D/MG3S, SOGGA/MG3S, MOHLYP/MG3S, and M08-SO/MG3S, respectively (therefore, the magenta and black horizontal lines are hard to distinguish visually because they are almost on top of one another).

predict a finite-distance transition state for any of the low-barrier reactions are excluded from the plot. The figure shows that there is indeed a correlation of error in bond length with error in barrier height if one compares density functional methods to one another or if one compares wave function methods to one another, but for a given accuracy in barrier heights, wave function methods predict more accurate transition state geometries. This is perhaps surprising since a strategy employed by many workers (including us) since the early days of DFT applications in chemistry has been to use DFT for geometries and WFT for energies, but one should keep in mind that the reason for using DFT for geometries is its lower cost. One can obtain more accurate geometries for a given cost with DFT.

Although the methods that failed to predict a finite-distance TS for any of the low-barrier reactions are left out of Figure 1, they generally also follow the correlation of large errors in barrier heights being associated with large errors in transition state geometries in that they have high average errors for the reactions where they do predict a transition state, and except for MOHLYP, they have high MUEs in barrier heights. For example, BLYP and SOGGA have MUEs for DBH24/08 of 8−10 kcal/mol.

For the reactions with a low reaction barrier, functionals that usually underestimate barrier heights are not well suited to locating transition state geometries. As already mentioned, reaction R15 is a good example of this, and it is interesting to further examine this case. The reaction is endoergic, and the barrier in the reverse direction is therefore the intrinsic barrier. Given that the barrier height for the reverse of R15 is quite small,[62,63] it is no surprise that it has vanished completely in calculations using density functionals like BLYP, B97-D, SOGGA, and MOHLYP that tend to significantly underestimate barrier heights; i.e., the potential energy decreases monotonically for the reverse reaction. To illustrate the shape of the energy profile in these cases, potential energy curves $V(\Delta_R)$, where Δ_R is a reaction coordinate defined below, were generated for reaction R15 by single-point BLYP/MG3S, B97-D/MG3S, SOGGA/MG3S, and MOHLYP/MG3S energy calculations along a fixed reaction path. The fixed reaction path corresponds to the M08-SO/MG3S minimum-energy path (MEP). The results are plotted as functions of Δ_R, which is defined as

$$\Delta_R \equiv \begin{cases} R_1 - R_1' & \text{before the saddle} \\ R_2' - R_2 & \text{after the saddle} \end{cases}$$

where R_1' and R_2' respectively correspond to the values (in angstroms) for the forming bond and the breaking bond for nonstationary points along the M08-SO/MG3S MEP. We have chosen M08-SO/MG3S to construct the MEP because this electronic model chemistry has been shown to accurately characterize the reaction energetics for hydrogen atom transfer reactions involving similar oxygenated hydrocarbons.[64] In each case, the potential curve was normalized relative to its value for the reactants. In addition, the reaction energy for R15 was also

Table 5. The Mean Unsigned Deviations (MUD, in Å) of Transition State Geometries for the Four Selected Reactions in TSG48 Database, Compared to the Best Estimated Geometries from refs 2 and 28 for the Three Wave Function Methods and Five Best DFT Methods over 16 Reactions in Table 3

method	R2[a]	R5[b]	R7[c]	R12[d]	AMUD[e]
BMC-CCSD	0.002	0.007	0.003	0.007	0.005
MRMP2/*nom*-CPO/MG3S[40]	0.011	0.003	0.004	0.009	0.007
QCISD/MG3	0.017	0.008	0.023	0.003	0.013
MC3BB	0.012	0.012	0.009	0.016	0.012
MC3MPW	0.016	0.014	0.013	0.015	0.014
M06−2X/MG3S	0.024	0.009	0.006	0.025	0.016
M08-HX/MG3S	0.040	0.011	0.000	0.025	0.019
M08-SO/MG3S	0.024	0.011	0.030	0.022	0.022

[a] Accurate values from ref 28b. [b] Accurate values from refs 28a. [c] Accurate values from ref 2. [d] Accurate values from ref 28c. [e] Average deviation from 12 accurate transition state internuclear distances.

calculated with each of the five density functional methods. The results of this analysis are depicted in Figure 2.

Figure 2 shows that while the TS for M08-SO/MG3S is higher in energy than that for the products (as expected), the reaction-path potential energies computed by the BLYP/MG3S, B97-D/MG3S, and SOGGA/MG3S electronic model chemistries are all significantly lower than that of the products. In the case of MOHLYP/MG3S, there are a few points along the potential energy curve that are slightly (up to 0.14 kcal/mol) higher in energy than the products. Interestingly, the potential curves obtained with BLYP/MG3S, B97-D/MG3S, MOHLYP/MG3S, and SOGGA/MG3S show mildly oscillatory behavior. In each of these cases, attempts were made to locate saddle points for R15 using the geometries of the higher-energy points as initial guesses as well as other initial geometry guesses, but no saddle points were found—we concluded that there is no saddle point in these cases. This illustrates how, for reactions with low intrinsic barriers, density functionals that tend to appreciably underestimate barrier heights not only are unsuitable for quantitative calculations of saddle point geometries, but, in some cases, fail to even predict the existence of a saddle point.

4.5. Comparison to MRMP2. The methods tested so far are single-reference methods, which are more convenient than multi-reference methods. One additional issue that is worth discussing, therefore, is whether it is advantageous to use multireference methods for even greater accuracy. It is well-known that complete-active-space self-consistent-field (CASSCF) theory[65,66] does not provide a reliable scheme for calculating transition state geometries because it neglects dynamical correlation energy. The next multireference level in terms of higher cost and higher accuracy is multireference second-order perturbation theory based on a CASSCF reference state. There is more than one version of this approach (e.g., MRMP2[67] and CASPT2[68]), and they are expected to give similar results if a similar selection is made for the active space. In recent work,[40] a well-defined choice of active space for atom transfer reactions, called the nominal correlated participating orbitals scheme (*nom*-CPO), was presented and used to optimize four of the transition states considered here for which we have more accurate results than BMC-CCSD. The mean unsigned deviations from the benchmark results and the average mean unsigned deviations from the benchmark results are presented in Table 5, where they are compared with the seven most accurate methods tested in earlier sections of this paper.

Table 5 shows that BMC-CCSD and MRMP2/*nom*-CPO have AMUDs in the 0.005−0.007 Å range, whereas the best of the other methods tested have AMUDs no smaller than 0.012 Å for these four reactions. Thus, we recommend both BMC-CCSD and MRMP2/*nom*-CPO when one wants higher accuracy than is afforded by MC3BB and M08-HX.

5. CONCLUDING REMARKS

In the present work, a database called TSG48 containing 48 transition state geometrical data for 16 reactions is introduced to assess the performance of density functionals for locating transition state geometries. The MC3BB and MC3MPW doubly hybrid functionals and the M08-HX and M06-2X hybrid meta-GGAs are found to have the best performance. M08-HX is the most highly recommended functional due to the excellent performance for all five subsets of TSG48, as well as having a lower cost when compared to doubly hybrid functionals. Functionals with good performance for barrier heights usually predict accurate transition state geometries, and similarly, bad performance for barrier heights is associated with less reliable prediction of transition state structures. Therefore, all local functionals tested in the present work, in particular, GGAs and meta-GGAs, and some hybrid density functionals, such as B97-D, τHCTHhyb, B3LYP, B1LYP, B98, and M05, are not recommended for locating transition states due to errors in geometry associated in part with the underestimation of the barrier height.

Due to a cancellation of errors, the 6-31+G(d,p) basis set gives better results than large basis sets for MP2, but 6-31+G(d,p) is not good enough for the best performance attainable with DFT methods. A minimally augmented triple-ζ basis set, such as MG3S, ma-TZVP, or maug-cc-pV(T+d)Z, is recommended.

AUTHOR INFORMATION

Corresponding Author

*E-mail: truhlar@umn.edu.

ACKNOWLEDGMENT

The authors are grateful to Jingjing Zheng for helpful assistance. This work was supported in part by the U.S. Department of Energy, Office of Science, Office of Basic Energy Sciences, under grant no. DE-FG02-86ER13579, and as part of the Combustion Energy Frontier Research Center under Award Number DE-SC0001198.

GLOSSARY

Density Functionals

See the last 34 rows of Table 2 for a list of density functionals included in the present study; references for these density functionals are cited at their first mention in the text in sections 1 and 3

Types of Density Functionals

GGA — generalized gradient approximation to the density functional, which is a type of density functional in which the exchange-correlation energy density at a point in space depends on the local values of the up-spin and down-spin electron densities and their reduced gradients

m — meta generalized gradient approximation to the density functional, which is like a GGA but the

	exchange-correlation energy density at a point in space also depends on the local values of the up-spin and down-spin electron kinetic energy densities
H	hybrid GGA in which the exchange energy also has a nonlocal component, which is Hartree−Fock exchange in the cases considered in this article
H−m	hybrid meta-GGA in which the exchange energy also has a nonlocal component, which is Hartree−Fock exchange in the cases considered in this article
DHDFT	doubly hybrid density functional, which is like a hybrid functional with the addition of a nonlocal component to the correlation energy as well as the exchange energy. In the cases considered in this article, this is an orbital-dependent term with the form of the MP2 correlation energy, computed using either the Hartree−Fock orbitals or the Kohn−Sham orbitals, which are both functionals of the electron density

Basis Sets

References explaining basis sets are given in section 2

Databases

DBH24	original database of 24 diverse barrier heights, with subdatabases explained in Table 1
DBH24/08	database of 24 diverse barrier heights, with the same reactions and subdatabases as DBH24 but with the majority of the barrier heights updated in 2008
MHTG12	database of 12 transition state geometrical data for methanol hydrogen transfer data, in particular, internuclear distances involving atoms in breaking and making bonds at transition state structures of four reactions involving abstraction of H from methanol
TSG48	database of 48 transition state geometrical data, in particular, internuclear distances involving atoms in breaking and making bonds at transition state structures of 16 reactions, with MHTG12 and four other subdatabases explained in section 2

Wave Function Methods

BMC-CCSD	balanced multicoefficient method based on coupled cluster theory with single and double excitations and a basis set especially balanced for extrapolation; the coefficients are used to extrapolate toward the complete configuration interaction limit
CASPT2	MRMP2 based on a CASSCF reference state
CASSCF	complete-active-space self-consistent-field
MP2	Møller−Plesset second-order perturbation theory based on a single-configuration wave function as the zero-order reference state
MRMP2	multireference MP2, that is, second-order perturbation theory based on a multiple-configuration wave function as the zero-order reference state
nom-CPO	nominal correlated participating orbitals, which is a way to specify the active space for MRMP2
QCISD	quadratic configuration interaction with single and double excitations

Mean Errors

MUD	mean unsigned deviation (i.e., mean absolute value of the deviation) from most accurate available reference data
AMUD	average MUD, that is, average over all of the reactions in a database of the MUD for the three key internuclear distances of each reaction

REFERENCES

(1) Baker, J.; Muir, M.; Andzelm, J.; Scheiner, A. *ACS Symp. Ser.* **1996**, *629*, 342.
(2) Parthiban, S.; de Oliveira, G.; Martin, J. M. L. *J. Phys. Chem. A* **2001**, *105*, 895.
(3) Lynch, B. J.; Truhlar, D. G. *J. Phys. Chem. A* **2003**, *107*, 3898.
(4) Lynch, B. J.; Truhlar, D. G. *J. Phys. Chem. A* **2003**, *107*, 8996.
(5) Guner, V.; Khuong, K. S.; Leach, A. G.; Lee, P. S.; Bartberger, M. D.; Houk, K. N. *J. Phys. Chem. A* **2003**, *107*, 11445.
(6) Zhao, Y.; Gonzalez-Garcia, N.; Truhlar, D. G. *J. Phys. Chem. A* **2005**, *109*, 2012.
(7) Ess, D. H.; Houk, K. N. *J. Phys. Chem. A* **2005**, *109*, 9542.
(8) Zheng, J.; Zhao, Y.; Truhlar, D. G. *J. Chem. Theory Comput.* **2007**, *3*, 569.
(9) Karton, A.; Tarnopolsky, A.; Lamre, J.-F.; Schatz, G. C.; Martin, J. M. L. *J. Phys. Chem. A* **2008**, *112*, 12868.
(10) Zheng, J.; Zhao, Y.; Truhlar, D. G. *J. Chem. Theory Comput.* **2009**, *5*, 808.
(11) Zhao, Y.; Truhlar, D. G. *J. Chem. Theory Comput.* **2008**, *4*, 1849.
(12) Zhao, Y.; Truhlar, D. G. *J. Chem. Phys.* **2006**, *125*, 194101.
(13) Zhao, Y.; Truhlar, D. G. *Theor. Chem. Acc.* **2008**, *120*, 215.
(14) Zhao, Y.; Lynch, B. J.; Truhlar, D. G. *J. Phys. Chem. A* **2004**, *108*, 2715.
(15) Boese, A. D.; Martin, J. M. L. *J. Chem. Phys.* **2004**, *121*, 3405.
(16) Zhao, Y.; Truhlar, D. G. *J. Phys. Chem. A* **2005**, *109*, 5656.
(17) Lynch, B. J.; Fast, P. L.; Harris, M.; Truhlar, D. G. *J. Phys. Chem. A* **2000**, *104*, 4811.
(18) (a) Becke, A. D. *Phys. Rev. A* **1988**, *38*, 3098. (b) Lee, C. T.; Yang, W. T.; Parr, R. G. *Phys. Rev. B* **1988**, *37*, 785. (c) Becke, A. D. *J. Chem. Phys.* **1993**, *98*, 1372.(d) Note that the BHandHLYP functional, explained in detail in the manual of the *Gaussian* computer program (ref 58), is similar in spirit to Becke's half-and-half functional of part c of this ref but not identical to it.
(19) Quintal, M. M.; Karton, A.; Iron, M. A.; Boese, A. D.; Martin, J. M. L. *J. Phys. Chem. A* **2006**, *110*, 709.
(20) Stephens, P. J.; Devlin, F. J.; Chabalowski, C. F.; Frisch, M. J. *J. Phys. Chem.* **1994**, *98*, 11623.
(21) Truhlar, D. G. *Faraday Discuss.* **1998**, *110*, 362.
(22) Adamo, C.; Barone, V. *J. Chem. Phys.* **1998**, *108*, 664.
(23) Lynch, B. J.; Truhlar, D. G. *J. Phys. Chem. A* **2001**, *105*, 2936.
(24) Pu, J.; Truhlar, D. G. *J. Phys. Chem. A* **2005**, *109*, 773.
(25) Zhao, Y.; Lynch, B. J.; Truhlar, D. G. *J. Phys. Chem. A* **2004**, *108*, 4786.
(26) Zhao, Y.; Truhlar, D. G. *Acc. Chem. Res.* **2008**, *41*, 157.
(27) Zhao, Y.; Truhlar, D. G. *Chem. Phys. Lett.* **2011**, *502*, 1.
(28) (a) Bian, W.; Werner, H.-J. *J. Chem. Phys.* **2000**, *112*, 220. (b) Peterson, K. A.; Dunning, T. H., Jr. *J. Phys. Chem. A* **1997**, *101*, 6280. (c) Van Mourik, T.; Harris, G. J.; Polyansky, O. L.; Tennyson., J.; Császár, A.; Knowles, P. *J. Chem. Phys.* **2001**, *115*, 3706. (d) Brown, F. B.; Truhlar, D. G. *Chem. Phys. Lett.* **1985**, *117*, 307. (e) Schwenke, D. W.; Tucker, S. C.; Steckler, R.; Brown, F. B.; Lynch, G. C.; Truhlar, D. G.; Garrett, B. C. *J. Chem. Phys.* **1989**, *90*, 3110.
(29) Lynch, B. J.; Zhao, Y.; Truhlar, D. G. *J. Phys. Chem. A* **2005**, *109*, 1643.
(30) Hirao, K. *Quantum Chem. Int. J.* **1992**, 517. Hirao, K. *Chem. Phys. Lett.* **1992**, *196*, 397.
(31) (a) Krishnan, R.; Binkley, J. S.; Seeger, R.; Pople, J. A. *J. Chem. Phys.* **1980**, *72*, 650. (b) Clark, T.; Chandrasekhar, J.; Spitznagel, G. W.;

Schleyer, P. v. R. *J. Comput. Chem.* **1983**, *4*, 294. (c) Frisch, M. J.; Pople, J. A.; Binkley, J. S. *J. Chem. Phys.* **1984**, *80*, 3265. (d) Curtiss, L. A.; Raghavachari, K.; Redfern, C.; Rassolov, V.; Pople, J. A. *J. Chem. Phys.* **1998**, *109*, 7764. (e) Fast, P. L.; Sanchez, M. L.; Truhlar, D. G. *Chem. Phys. Lett.* **1999**, *306*, 407. (f) Lynch, B. J.; Zhao, Y.; Truhlar, D. G. *J. Phys. Chem. A.* **2003**, *107*, 1384.

(32) (a) Kendall, R. A.; Dunning, T. H., Jr.; Harrison, R. J. *J. Chem. Phys.* **1992**, *96*, 6796. (b) Woon, D. E.; Dunning, T. H., Jr. *J. Chem. Phys.* **1993**, *98*, 1358.

(33) Pople, J. A.; Head-Gordon, M.; Raghavachari, K. *J. Chem. Phys.* **1987**, *87*, 5968.

(34) Tratz, C.; Fast, P. L.; Truhlar, D. G. *Phys. Chem. Comm.* **1999**, *2*, 14.

(35) Møller, C.; Plesset, M. S. *Phys. Rev.* **1934**, *46*, 618.

(36) Zheng, J.; Xu, X.; Truhlar, D. G. *Theor. Chem. Acc.* **2011**, *128*, 295.

(37) Weigend, F.; Ahlrichs, R. *Phys. Chem. Chem. Phys.* **2005**, *7*, 3297.

(38) (a) Dunning, T. H., Jr. *J. Chem. Phys.* **1989**, *90*, 1007. (b) Papajak, E.; Leverentz, H. R.; Zheng, J.; Truhlar, D. G. *J. Chem. Theory Comput.* **2009**, *5*, 1197.

(39) (a) Hariharan, P. C.; Pople, J. A. *Theor. Chem. Acta* **1973**, *28*, 213. (b) Francl, M. M.; Pietro, W. J.; Hehre, W. J.; binkley, J. S.; Gordon, M. S.; DeFrees, D; Pople, J.; Pople, A. *J. Chem. Phys.* **1982**, *77*, 3654.

(40) Tishchenko, O.; Zheng, J.; Truhlar, D. G. *J. Chem. Theory Comput.* **2008**, *4*, 1208.

(41) Schultz, N.; Zhao, Y.; Truhlar, D. G. *J. Phys. Chem. A* **2005**, *109*, 11127.

(42) Zhao, Y.; Truhlar, D. G. *J. Chem. Phys.* **2008**, *128*, 184109.

(43) Chai, J.-D.; Head-Gordon, M. *J. Chem. Phys.* **2008**, *128*, 084106.

(44) Chai, J.-D.; Head-Gordon, M. *Phys. Chem. Chem. Phys.* **2008**, *10*, 6615.

(45) (a) Perdew, J. P.; Burke, K.; Ernzerhof, M. *Phys. Rev. Lett.* **1996**, *77*, 3865. (b) Adamo, C.; Cossi, M.; Barone, V. *THEOCHEM* **1999**, *493*, 145.

(46) Keal, T. W.; Tozer, D. J. *J. Chem. Phys.* **2005**, *123*, 121103.

(47) Grimme, S. *J. Comput. Chem.* **2006**, *27*, 1787.

(48) Schmider, H. L.; Becke, A. D. *J. Chem. Phys.* **1998**, *108*, 9624.

(49) Adamo, C.; Barone, V. *Chem. Phys. Lett.* **1997**, *274*, 242.

(50) Zhao, Y.; Truhlar, D. G. *J. Phys. Chem. A* **2004**, *108*, 6908.

(51) Zhao, Y.; Schultz, N. E.; Truhlar, D. G. *J. Chem. Theory Comput.* **2006**, *2*, 364.

(52) Zhao, Y.; Truhlar, D. G. *J. Phys. Chem. A* **2006**, *110*, 13126.

(53) Zhao, Y.; Schultz, N. E.; Truhlar, D. G. *J. Chem. Phys.* **2005**, *123*, 161103.

(54) Boese, A. D.; Handy, N. C. *J. Chem. Phys.* **2002**, *116*, 9559.

(55) Grimme, S. *J. Chem. Phys.* **2006**, *124*, 034108.

(56) Frisch, M. J.; Trucks, G. W.; Schlegel, H. B.; Scuseria, G. E.; Robb, M. A.; Cheeseman, J. R.; Scalmani, G.; Barone, V.; Mennucci, B.; Petersson, G. A.; Nakatsuji, H.; Caricato, M.; Li, X.; Hratchian, H. P.; Izmaylov, A. F.; Bloino, J.; Zheng, G.; Sonnenberg, J. L.; Hada, M.; Ehara, M.; Toyota, K.; Fukuda, R.; Hasegawa, J.; Ishida, M.; Nakajima, T.; Honda, Y.; Kitao, O.; Nakai, H.; Vreven, T.; Montgomery, J. A., Jr.; Peralta, J. E.; Ogliaro, F.; Bearpark, M.; Heyd, J. J.; Brothers, E.; Kudin, K. N.; Staroverov, V. N.; Kobayashi, R.; Normand, J.; Raghavachari, K.; Rendell, A.; Burant, J. C.; Iyengar, S. S.; Tomasi, J.; Cossi, M.; Rega, N.; Millam, N. J.; Klene, M.; Knox, J. E.; Cross, J. B.; Bakken, V.; Adamo, C.; Jaramillo, J.; Gomperts, R.; Stratmann, R. E.; Yazyev, O.; Austin, A. J.; Cammi, R.; Pomelli, C.; Ochterski, J. W.; Martin, R. L.; Morokuma, K.; Zakrzewski, V. G.; Voth, G. A.; Salvador, P.; Dannenberg, J. J.; Dapprich, S.; Daniels, A. D.; Farkas, Ö.; Foresman, J. B.; Ortiz, J. V.; Cioslowski, J.; Fox, D. J. *Gaussian 09*, Revision A.02; Gaussian, Inc.: Wallingford, CT, 2009.

(57) Frisch, M. J.; Trucks, G. W.; Schlegel, H. B.; Scuseria, G. E.; Robb, M. A.; Cheeseman, J. R.; Scalmani, G.; Barone, V.; Mennucci, B.; Petersson, G. A.; Nakatsuji, H.; Caricato, M.; Li, X.; Hratchian, H. P.; Izmaylov, A. F.; Bloino, J.; Zheng, G.; Sonnenberg, J. L.; Hada, M.; Ehara, M.; Toyota, K.; Fukuda, R.; Hasegawa, J.; Ishida, M.; Nakajima, T.; Honda, Y.; Kitao, O.; Nakai, H.; Vreven, T.; Montgomery, J. A., Jr.; Peralta, J. E.; Ogliaro, F.; Bearpark, M.; Heyd, J. J.; Brothers, E.; Kudin, K. N.; Staroverov, V. N.; Kobayashi, R.; Normand, J.; Raghavachari, K.; Rendell, A.; Burant, J. C.; Iyengar, S. S.; Tomasi, J.; Cossi, M.; Rega, N.; Millam, N. J.; Klene, M.; Knox, J. E.; Cross, J. B.; Bakken, V.; Adamo, C.; Jaramillo, J.; Gomperts, R.; Stratmann, R. E.; Yazyev, O.; Austin, A. J.; Cammi, R.; Pomelli, C.; Ochterski, J. W.; Martin, R. L.; Morokuma, K.; Zakrzewski, V. G.; Voth, G. A.; Salvador, P.; Dannenberg, J. J.; Dapprich, S.; Daniels, A. D.; Farkas, Ö.; Foresman, J. B.; Ortiz, J. V.; Cioslowski, J.; Fox, D. J. *Gaussian 03*, Revision D.01; Gaussian, Inc.: Wallingford, CT, 2003.

(58) (a) Frisch, M. J.; Trucks, G. W.; Schlegel, H. B.; Scuseria, G. E.; Robb, M. A.; Cheeseman, J. R.; Scalmani, G.; Barone, V.; Mennucci, B.; Petersson, G. A.; Nakatsuji, H.; Caricato, M.; Li, X.; Hratchian, H. P.; Izmaylov, A. F.; Bloino, J.; Zheng, G.; Sonnenberg, J. L.; Hada, M.; Ehara, M.; Toyota, K.; Fukuda, R.; Hasegawa, J.; Ishida, M.; Nakajima, T.; Honda, Y.; Kitao, O.; Nakai, H.; Vreven, T.; Montgomery, J. A., Jr.; Peralta, J. E.; Ogliaro, F.; Bearpark, M.; Heyd, J. J.; Brothers, E.; Kudin, K. N.; Staroverov, V. N.; Kobayashi, R.; Normand, J.; Raghavachari, K.; Rendell, A.; Burant, J. C.; Iyengar, S. S.; Tomasi, J.; Cossi, M.; Rega, N.; Millam, N. J.; Klene, M.; Knox, J. E.; Cross, J. B.; Bakken, V.; Adamo, C.; Jaramillo, J.; Gomperts, R.; Stratmann, R. E.; Yazyev, O.; Austin, A. J.; Cammi, R.; Pomelli, C.; Ochterski, J. W.; Martin, R. L.; Morokuma, K.; Zakrzewski, V. G.; Voth, G. A.; Salvador, P.; Dannenberg, J. J.; Dapprich, S.; Daniels, A. D.; Farkas, Ö.; Foresman, J. B.; Ortiz, J. V.; Cioslowski, J.; Fox, D. J. *Gaussian 03*, Revision E.01; Gaussian, Inc.: Wallingford, CT, 2003. (b) Zhao, Y.; Truhlar, D. G. *MN-GFM: Minnesota Gaussian Functional Module*, version 4.1; University of Minnesota: Minneapolis, MN, 2008.

(59) Zhao, Y. Truhlar, D. G. *MLGAUSS*, version 2.0; University of Minnesota: Minneapolis, MN, 2006.

(60) Lynch, B. J.; Zhao, Y.; Truhlar, D. G. *J. Phys. Chem. A* **2003**, *107*, 1384.

(61) Papajak, E.; Truhlar, D. G. *J. Chem. Theory Comput.* **2010**, *6*, 597.

(62) Klippenstein, S. J.; Harding, L. B.; Davis, M. J.; Tomlin, A. S.; Skodje, R. T. *Proc. Combust. Inst.* **2011**, *33*, 351.

(63) Skodje, R. T.; Tomlin, A. S.; Klippenstein, S. J.; Harding, L. B.; Davis, M. J. *J. Phys. Chem. A* **2010**, *114*, 8286.

(64) Zheng, J.; Truhlar, D. G. *Phys. Chem. Chem. Phys.* **2010**, *12*, 7782.

(65) Ruedenberg, K.; Sundberg, K. R. In *Quantum Science: Methods and Strcuture*; Calais, J.-L., Goscinski, O., Linderberg, J., Ohrn, Y., Eds.; Plenum: New York, 1976; p 505.

(66) Roos, B. O.; Taylor, P. R.; Siegbahn, P. E. M. *Chem. Phys.* **1980**, *48*, 157.

(67) Nakano, H.; Nakajima, T.; Tsuneda, T.; Hirao, K. In *Theory and Applications of Computational Chemistry: The First Forty Years*; Dykstra, C. E., Frenking, G., Kim, K. S., Scuseria, G. E., Eds.; Elsevier: Amsterdam, 2005; p 507.

(68) Roos, B. O. In *Theory and Applications of Computational Chemistry: The First Forty Years*; Dykstra, C. E., Frenking, G., Kim, K. S., Scuseria, G. E., Eds.; Elsevier: Amsterdam, 2005; p 725.